Temperature and electric-field induced phase transitions, and full tensor properties of $[011]_C$-poled domain-engineered tetragonal $0.63Pb(Mg_{1/3}Nb_{2/3})$-$0.37PbTiO_3$ single crystals

Limei Zheng,[1] Yujia Jing,[1] Xiaoyan Lu,[2] Ruixue Wang,[1] Gang Liu,[3] Weiming Lü,[1] Rui Zhang,[1] and Wenwu Cao[1,4,*]

[1]*Condensed Matter Science and Technology Institute, Harbin Institute of Technology, Harbin 150080, China*

[2]*Key Laboratory of Structures Dynamic Behavior and Control of the Ministry of Education, School of Civil Engineering, Harbin Institute of Technology, Harbin 150001, China*

[3]*Center for High Pressure Science and Technology Advanced Research, Shanghai 201203, China*

[4]*Department of Mathematics, Materials Research Institute, The Pennsylvania State University, University Park, Pennsylvania 16802, USA*

(Received 7 December 2015; revised manuscript received 18 February 2016; published 14 March 2016)

The phase-transition sequence of $0.67Pb(Mg_{1/3}Nb_{2/3})-0.37PbTiO_3$ (PMN-0.37PT) single crystals driven by the electric (E) field and temperature is comprehensively studied. Based on the strain-E field loop, polarization-E field loop, and the evolution of domain configurations, the E field along the $[011]_C$ induced phase transitions have been confirmed to be as follows: tetragonal (T) $\rightarrow$ monoclinic (M_C) $\rightarrow$ single domain orthorhombic (O) phase. As the E field decreases, the induced O phase cannot be maintained and transformed to the M_C phase, then to the coexistence state of M_C and T phases. In addition, the complete sets of dielectric, piezoelectric, and elastic constants for the $[011]_C$-poled domain-engineered PMN-0.37PT single crystal were measured at room temperature, which show high longitudinal dielectric, piezoelectric, and electromechanical properties ($\varepsilon_{33}^T = 10\,661$, $d_{33} = 1052$ pC/N, and $k_{33} = 0.766$). Our results revealed that the M_C phase plays an important role in the high electromechanical properties of this domain-engineered single crystal. The temperature dependence of the domain configuration revealed that the volume fraction of the M_C phase decreases with temperature accompanied by the reduction of ε_{33}^T, d_{31}, and k_{31} due to the substantially smaller intrinsic properties of the T phase.

DOI: 10.1103/PhysRevB.93.094104

I. INTRODUCTION

Relaxor-based single crystals, such as $(1-x)Pb(Mg_{1/3}Nb_{2/3})$-$xPbTiO_3$(PMN-$x$PT), $(1-x)Pb(Zn_{1/3}Nb_{2/3})$-$xPbTiO_3$(PZN-$x$PT), and $(1-x)Pb(Sc_{1/3}Nb_{2/3})$-$xPbTiO_3$ (PSN-xPT) have been extensively studied in the past two decades due to their ultrahigh piezoelectric coefficients (>2000 pC/N), electromechanical coupling factors (>0.9),and low loss (<2%) [1–5]. Such giant piezoelectricity has triggered a revolution in many electromechanical devices, including medical ultrasonic imaging transducers, actuators, sonars, accelerometers, etc. Among all relaxor-based single crystals, the PMN-x PT single crystal is the most widely used due to its broad morphotropic-phase boundary (MPB) and easy growth characteristics [6]. So far, most researchers focused their interests on the rhombohedral (R) phase or MPB composition crystals, whereas few studies were carried out on the tetragonal- (T-) phase crystals. The T-phase crystal shows a higher Curie temperature T_C than the R phase or the MPB composition, therefore, one would expect a wider temperature usage range because no phase transition occurs between room temperature and T_C [7,8]. Also, it was demonstrated that the T-phase crystal showed high piezoelectric coefficients and electromechanical coupling factors in its domain-engineered structures [9]. However, detailed piezoelectric properties and the E field and temperature dependence of the T-phase PMN-PT single crystals have not been fully studied to date. In fact, there is not even one complete set of material constants for the domain-engineered tetragonal PMN-PT system in the literature. For fundamental studies and device designs, a comprehensive study on the phase stability, full tensor properties, and the temperature-dependent electric properties of a domain-engineered T-phase PMN-x PT single crystal is highly desired. There are also some rich physical phenomena involved in the structural phase transitions.

In this paper, we focus on the T phase of the PMN-0.37PT single crystal with the composition not very far away from the MPB. The phase-transition behavior under an E field along $[011]_C$ was studied, and a complete set of dielectric, piezoelectric, and elastic constants for the $[011]_C$-poled domain-engineered single crystals was determined. The temperature dependence of piezoelectric and electromechanical properties was also studied, and their variations were correlated with the change in microstructure and intrinsic contributions of coexisting phases.

II. EXPERIMENTAL PROCEDURE

The single crystal (TRS Technologies, USA) was grown by the modified Bridgman method and was oriented by the x-ray diffraction method. Gold films were sputtered onto the desired surfaces as electrodes. All samples were poled at room temperature along $[011]_C$ using a dc field of 8 kV/cm and then were aged for a period of 2–30 days to wait for the properties to become stable before measurements were performed. The full tensor properties of the $[011]_C$-poled PMN-0.37PT samples were determined by the combined resonance and ultrasonic method, and the details of the method can be found in Refs. [10,11]. The resonance and antiresonance frequencies were measured by an Agilent 4294A impendence-phase analyzer. Polarization-E-field hysteresis loops (P-E loops) and electric-field induced strain loops (S-E loops) were

*Corresponding author: dzk@psu.edu

measured at the frequency of 1 Hz using a Premier II Precision Materials Analyzer (Radiant Technologies, Inc., Albuquerque, NM). The temperature dependence of dielectric permittivity was measured using a multifrequency LCR meter, which was connected to a computer-controlled furnace. The domain structures were observed by a polarizing light microscope (Zessi Sxiokop40). For domain observations, the two $(100)_C$ surfaces of the samples were polished into optical quality, and gold films were sputtered onto the $(100)_C$ and $(0\bar{1}\bar{1})_C$ surfaces as electrodes. During the *in situ* observation of the domain configurations, an E field was applied along $[011]_C$, and the domain structures were observed along $[100]_C$. Details of the domain observation procedure by polarizing light microscopy (PLM) can be referred to in Ref. [1].

III. RESULTS AND DISCUSSION

A. Phase transitions driven by an E field

For the tetragonal ferroelectric structure, the crystallographic symmetry is $4mm$. There are six possible spontaneous polarizations (P_S) along the six equivalent $\langle 001\rangle_C$ directions as shown in Fig. 1(a). Under an E field along $[011]_C$, if no phase transition is being induced, the polarizations tend to switch to the two directions closest to the E-field direction, i.e., $[001]_C$ and $[010]_C$ as shown in Fig. 1(b). However, if phase transitions are induced, P_S will rotate to directions other than these six directions, resulting in unusual dielectric and mechanical behaviors. Therefore, before the determination of material constants, it is important to reveal the phase-transition sequence as a function of the E field, the temperature, and the rotation paths of P_S vectors under a specified E field.

Figure 2 shows the S-E loops for the $[011]_C$-poled sample. Two inflection points at around 4 and 6 kV/cm can be observed with the increase in the E field, corresponding to two phase transitions. The converse piezoelectric constant d_{33}^* in the three intervals can be obtained by a linear fitting of the S-E curve, which are determined to be 1336 pm/V($E < 4$ kV/cm),4645 pm/V (4 kV/cm $< E <$ 6 kV/cm), and 177 pm/V($E >$ 6kV/cm), respectively. The piezoelectric response above 6 kV/cm is very low, comparable to that of the single domain state [5,12,13] at which the piezoelectric effect only comes from P_S extension without polarization rotation [14,15]. The phase structure in this region should be single domain orthorhombic (O) with the P_S along $[011]_C$, the same direction as the applied E field.

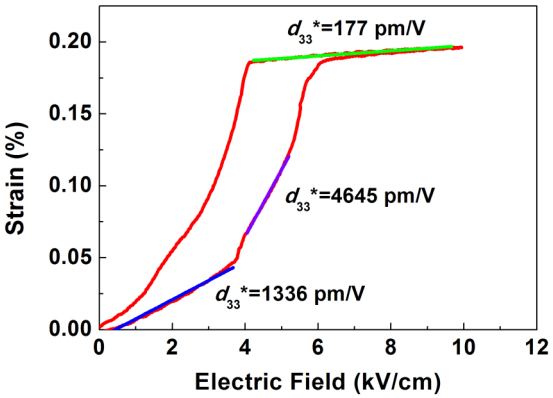

FIG. 2. Strain-electric field loops for the $[011]_C$-orientated PMN-0.37PT single crystal.

The piezoelectric response in the interval of 4 kV/cm $< E <$ 6 kV/cm is extremely high. One can infer that the phase structure in this region might be monoclinic in which the P_S vectors can rotate continuously under an E field so that an extremely high piezoelectric response can be obtained [16–19]. Two kinds of monoclinic phases have been reported in the PMN-xPT system: the M_A phase with Cm symmetry and the M_C phase with Pm symmetry [20–22]. There are 24 polarizations in both M_A and M_C phases. But the P_S directions are different. In the M_A phase, polarizations are confined to the $\{110\}_C$ planes, whereas those in M_C phase are confined to the $\{100\}_C$ planes as shown in Figs. 3(a) and 3(b). Based on Fig. 2, it is difficult to discern whether it is the M_A phase or the M_C phase. It can be seen that the P_S vectors of the M_C phase lie in between two adjacent P_S vectors of the T and O phases. That is to say, P_S can rotate continuously from tetragonal $[001]_C$ to orthorhombic $[011]_C$ through the M_C phase, the P_S directions of O and T phases are connected through the M_C phase. So we may conclude that the monoclinic phase is M_C, not M_A.

During the decreasing process of the E field, the single domain O phase returns to the M_C phase at around 4 kV/cm where extremely high piezoelectricity can be obtained. No obvious phase transition can be observed below 4 kV/cm, and the d_{33}^* value reduces gradually with the decrease in the E field. Based on the above information alone, it is difficult to determine the phase structure after the removal of the E field.

In order to further investigate the rotation of P_S vectors under the E field, the hysteresis loop (P-E loop) of $[011]_C$-

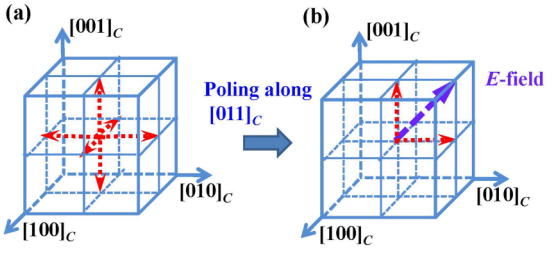

FIG. 1. Schematic of spontaneous polarizations in the perovskite tetragonal phase: (a) six polarizations along $\langle 001\rangle_C$ families before poling and (b) after being poled along $[011]_C$ and only two polarizations along $[001]_C$ and $[010]_C$ are left.

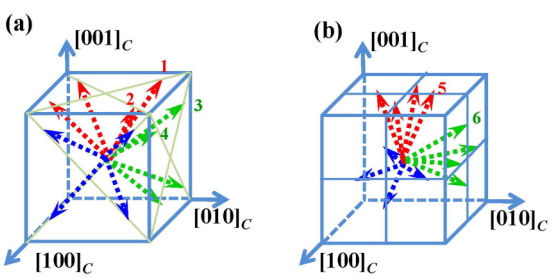

FIG. 3. Schematic of possible P_S vectors in the (a) M_A phase and (b) M_C phases. Here we only illustrate 12 of the 24 P_S directions, and the other 12 P_S are opposites of these 12 directions.

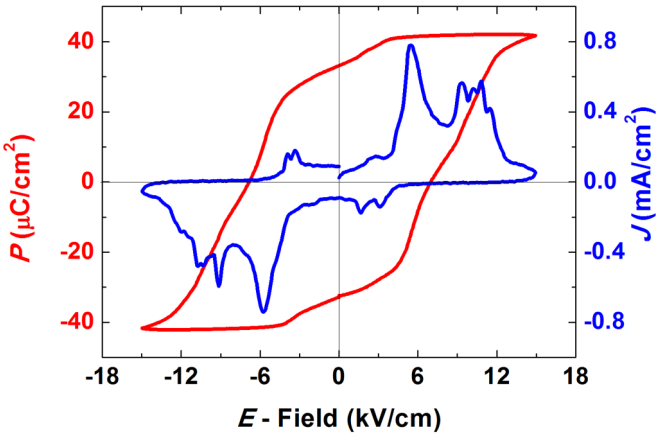

FIG. 4. *P-E* loops and derived *J-E* curves for the $[011]_C$-orientated PMN-0.37PT single crystal.

oriented PMN-0.37PT single crystals was measured, and the *E*-field dependence of the current density *J* was derived as shown in Fig. 4. The *E*-field induced phase transitions are also reflected in the *P-E* loop and the *J-E* curve. The current peak at ~5.5 kV/cm in the *J-E* curve corresponds to the switching of polarizations in the same phase. With the increase in the *E* field, two other *J* peaks can be observed at around 9.3 and 10.8 kV/cm, respectively. These two peaks correspond to the two field induced phase transitions as shown in Fig. 2. During this process, the P_S vectors rotate continuously from their original directions to the final $[011]_C$ directions through the M_C phase paths, so the *J* peaks in this interval are broad and may be composed of many small peaks. During the decreasing in the *E* field, a *J* peak corresponding to the *O*-M_C phase transition can be observed at around 3.8 kV/cm, consistent with the results in Fig. 2.

From Fig. 4, the residual polarization P_r is 33.0 μC/cm^2. The P_S of the *T* phase for this PMN-0.37PT single crystal determined from the *P-E* loop of the $[001]_C$-oriented sample (not shown here) is 40.1 μC/cm^2. If the phase structure returns to the pure *T* phase when the *E* field decreases to 0 kV/cm, there should be only P_S vectors along $[001]_C$ and $[010]_C$, so the theoretical residual polarization P_{rt} of the $[011]_C$-oriented samples may be calculated by

$$P_{rt} = \frac{P_s}{\sqrt{2}} = 28.5\,\mu\text{C/cm}^2. \quad (1)$$

This value is much smaller than the measured 33.0 μC/cm^2. So the phase structure at $E = 0$ kV/cm is not a pure *T* phase but the coexistence of both *T* and *M* phases. In order to accurately identify the phase structure in each interval, the *in situ* observation of domain evolution with the *E* field along $[011]_C$ was carried out by PLM, and the results are shown in Fig. 5. Based on the extinction positions and the directions of the domain walls, the phase structure can be deduced. During the observation, the angle between the polarizer and the $[001]_C$ direction of the sample is defined as θ. Before the application of the *E* field, the sample possesses typical domain structures of the *T* phase, showing maximum transmitted light intensity at $\theta = 45°$ and extinction at 0° [Figs. 5(a) and 5(b)]. The *T* phase is maintained until $E = 5$ kV/cm at which the

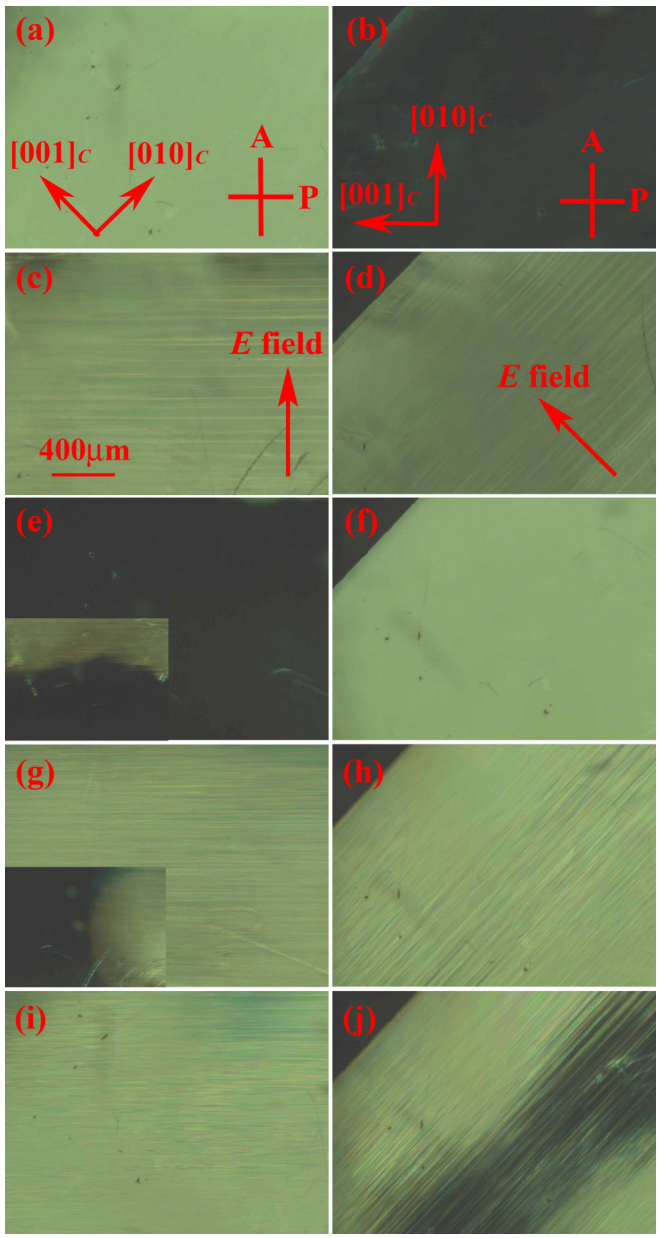

FIG. 5. Domain structures at room temperture with a dc *E* field applied along $[011]_C$. (a) and (b) 0 kV/cm, (c) and (d) 5 kV/cm, (e) and (f) 7 kV/cm during the field increasing process, (g) and (h) 3.5 kV/cm, and (i) and (j) 0 kV/cm during the field decreasing process. Images in the left column were taken at $\theta = 45°$, whereas those in the right column were taken at $\theta = 0°$.

domain structure undergoes an abrupt change, indicating that a phase transition occurred. The new phase does not show complete extinction as θ changes from 0° to 90° [Figs. 5(c) and 5(d)], and the domain walls are along $[0\bar{1}1]_C$. As mentioned above, the new phase should be an *M* phase. For the M_C phase, two P_S vectors closest to $[011]_C$ would be left [P_S denoted by 5 and 6 in Fig. 3(b)] under an *E* field along $[011]_C$, whereas there would be four P_S vectors left [P_S 1–4 in Fig. 3(a)] in the M_A phase. Considering the P_S directions of M_A and M_C phases and based on the analysis in our previous work, it is inferred that the domain wall of the $[011]_C$-poled

M_C phase is along $[0\bar{1}1]_C$, whereas that of the M_A phase should not lie in this direction when observed on the $(100)_C$ surface [1]. So the M_C phase is further confirmed. As the E field further increases to 7 kV/cm, another drastic change in domain structures was observed, corresponding to the M_C to O phase transition. The new phase shows complete extinction at $\theta = 45^\circ$ and maximum light intensity at $\theta = 0^\circ$, coinciding well with the characteristics of the single domain O phase with P_S along $[011]_C$ [Figs. 5(e) and 5(f)]. Therefore, the phase-transition sequence is $T \rightarrow M_C \rightarrow O$ with the increase in the E field.

When the E field decreases from its maximum value, the single domain O phase was maintained until the E field decreases down to 3.5 kV/cm at which point the O phase returns to the M_C phase [Figs. 5(g) and 5(h), the inset of Fig. 5(g) shows the domain image during the phase-transition process]. As the E field further decreases, dark regions begin to form as shown in Fig. 5(j), revealing the nucleation of T domains in the M_C matrix. The volume fraction of the T domain enlarges with the decrease in the E field, but the M_C phase does not vanish, so the phase structure at the 0-kV/cm field should be the coexistence of the T and M_C phases. The phase-transition sequence during the decreasing process of the E field is $O \rightarrow M_C \rightarrow M_C + T$. Polarization vectors in the $[011]_C$-poled PMN-0.37PT single crystal should be the mixture of P_S of these two phases, i.e., two P_S vectors of the T phase ($[001]_C$ and $[010]_C$) and two P_S vectors of the M_C phase (P_S 5 and 6 in Fig. 3), a total of four different types of polarizations. It is difficult to accurately measure the domain size for each phase in the coexisting phase structure using the available observation techniques, particularly for three-dimensional (3D) structures in which domain patterns overlap along the observation direction. Thinning down the crystal for TEM observation will totally change the boundary conditions so that the domain configuration will not reflect the true 3D domain patterns, whereas the resolution of PLM is too low to give an accurate measure because the domain size is very small as can be seen from the high domain-wall density in Figs. 5(i) and 5(j).

Figure 6 shows the domain structures of a $[011]_C$-poled PMN-0.37PT crystal after a few hours of aging. The opaque areas became larger with aging time, indicating the increase in the T-phase volume fraction, so the M_C phase is metastable without a field. After aging for 48 h, the domain structure and electrical properties do not show any more noticeable changes. All measurements in this paper were performed after an aging period between 2 and 30 days.

It should be noted that there are discrepancies in the phase-transition fields determined from the S-E loop, the P-E loop, and the domain observation. Many factors may contribute to these discrepancies, including the frequency of the driving E field and the poling history of the sample. A prepoled sample is used in the S-E loop measurements in which only phase-transition-related P_S rotation is involved, so the phase transitions can occur at a relatively lower E field. However, an unpoled sample is used in the P-E loop measurements for which the sample was first poled reversely in the previous cycle, whereas in the next cycle, the P_S vector first switched to a direction much closer to $[011]_C$ under a certain level of the E field, but no phase transition is involved. A further increase in the E field will result in phase transitions. So the threshold field in the P-E loop measurements is higher than that in the S-E loop. In the domain observations, a dc bias instead of an ac field is applied on an unpoled sample, thus, some of the P_S vectors will first switch,then phase transitions will occur. Compared to the P-E and S-E loop measurements where an ac E field is applied, P_S vectors and domain walls would have enough time to react under the dc field in the domain observation experiments, so the phase transition may occur under a lower field than that in the P-E loop but higher than in the S-E curve in which T-phase P_S switching is not involved [23].

To summarize, at room temperature, the unpoled PMN-0.37PT single crystal is in the T phase. It undergoes the transition sequence of $T \rightarrow M_C \rightarrow O$ under an E field along $[011]_C$. The single domain O phase cannot be maintained without the E field, and it transforms into the M_C phase and then to the coexistence of M_C and T phases as the E field decreases back to zero.

B. Full tensor properties of $[011]_C$-poled PMN-PT single crystals

Knowing the complete set of material constants of a crystal with a complex structure is of great importance from both application and fundamental research points of view. First of all, all material constants are macroscopic properties, and they are used for the practical design of devices. From a fundamental viewpoint, the knowledge on these properties sets a starting point for more detailed theoretical studies on the influence of microstructures to these macroscopic properties. Such full tensor properties also give us a quantified understanding on the anisotropic nature of the engineered domain structure. For this purpose, we have measured the full tensor properties of a $[011]_C$-poled PMN-0.37PT single crystal. After poling along $[011]_C$, the effective macroscopic symmetry of the multidomain crystal is orthorhombic $mm2$ regardless of the phase structures with a total of 17 independent material constants: 9 elastic constants, 5 piezoelectric constants, and 3

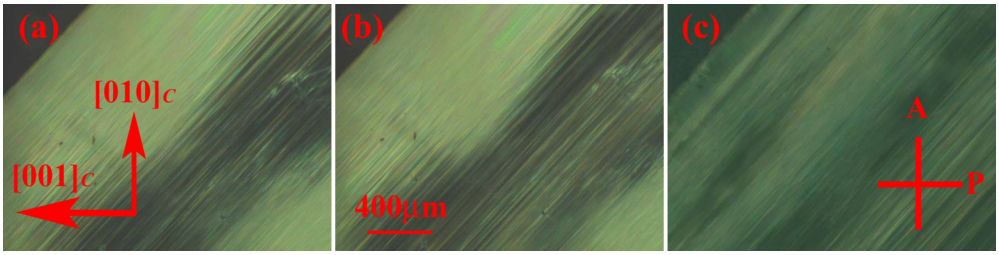

FIG. 6. Domain configrations of the $[011]_C$-poled PMN-0.37PT single crystal after aging times of (a) 0 min, (b) 15 min, and (c) 48 h.

TABLE I. Measured and derived material constants of a $[011]_C$-poled single domain PMN-0.37PT crystal (Density: $\rho = 8108\,\mathrm{kg/m^3}$).

Elastic stiffness constants: c_{ij}^E and $c_{ij}^D(10^{10}\,\mathrm{N/m^2})$											
c_{11}^E	c_{12}^E	c_{13}^E	c_{22}^E	c_{23}^E	c_{33}^E	c_{44}^E	c_{55}^E	c_{66}^E			
18.9	12.7	10.9	16.9	5.9	11.6	5.3	23.8	3.1			
c_{11}^D	c_{12}^D	c_{13}^D	c_{22}^D	c_{23}^D	c_{33}^D	c_{44}^D	c_{55}^D	c_{66}^D			
24.3	16.1	7.1	19.1	3.4	14.4	8.3	28.8	3.1			
Elastic compliance constants: s_{ij}^E and $s_{ij}^D(10^{-12}\,\mathrm{m^2/N})$											
s_{11}^E	s_{12}^E	s_{13}^E	s_{22}^E	s_{23}^E	s_{33}^E	s_{44}^E	s_{55}^E	s_{66}^E			
20.5	−10.5	−14.0	12.6	3.6	20.0	18.9	4.2	32.8			
s_{11}^D	s_{12}^D	s_{13}^D	s_{22}^D	s_{23}^D	s_{33}^D	s_{44}^D	s_{55}^D	s_{66}^D			
10.7	−8.5	−3.3	12.2	1.3	8.3	12.0	3.5	32.8			
Piezoelectric coefficients: $d_{i\lambda}(10^{-12}\,\mathrm{C/N})$, $e_{i\lambda}(\mathrm{C/m^2})$, $g_{i\lambda}(10^{-3}\,\mathrm{Vm/N})$, $h_{i\lambda}(10^8\,\mathrm{V/m})$											
d_{15}	d_{24}	d_{31}	d_{32}	d_{33}	e_{15}	e_{24}	e_{31}	e_{32}	e_{33}		
120	645	−960	204	1052	28.4	34.1	−40.4	−25.7	29.0		
g_{15}	g_{24}	g_{31}	g_{32}	g_{33}	h_{15}	h_{24}	h_{31}	h_{32}	h_{33}		
6.2	10.7	−10.2	2.2	11.2	17.7	8.9	−13.3	−8.5	9.5		
Dielectric constants: $\varepsilon_{ij}(\varepsilon_0)$ and $\beta_{ij}(10^{-4}/\varepsilon_0)$											
ε_{11}^T	ε_{22}^T	ε_{33}^T	ε_{11}^S	ε_{22}^S	ε_{33}^S	β_{11}^T	β_{22}^T	β_{33}^T	β_{11}^S	β_{22}^S	β_{33}^S
2197	6803	10 661	1812	4321	3430	4.55	1.47	0.94	5.52	2.31	2.92
Electromechanical coupling factors											
k_{15}	k_{24}	k_{31}	k_{32}	k_{33}	k_t						
0.418	0.604	0.691	0.187	0.766	0.439						

dielectric constants. We have measured these constants using combined resonance and pulse-echo techniques, and they are listed in Table I.

The $[011]_C$-poled PMN-0.37PT single crystal possesses high longitudinal properties ($\varepsilon_{33}^T = 10\,661, d_{33} = 1052\,\mathrm{pC/N}$, and $k_{33} = 0.766$) but relatively low transverse dielectric constants ($\varepsilon_{11}^T = 2197$ and $\varepsilon_{22}^T = 6803$) and shear piezoelectric properties ($d_{15} = 120\,\mathrm{pC/N}, k_{15} = 0.418, d_{24} = 645\,\mathrm{pC/N}$, and $k_{24} = 0.604$), which are typical characteristics of multidomain crystals in perovskite systems. The longitudinal dielectric constant of this domain-engineered T-phase crystal is much higher than that of the domain-engineered R and MPB compositions [24–26], whereas the longitudinal piezoelectricity is comparable to that of the domain-engineered R phase [5,27,28]. Our results here enriched the database in the literature to include the domain-engineered T phase. One can see from the obtained complete set of material constants that the $[011]_C$-poled tetragonal PMN-0.37PT single crystal is an excellent candidate for dielectric and electromechanical device applications.

The E-field induced phase transitions may strongly affect the physical properties of the material. As mentioned above, the PMN-0.37PT cannot return to a pure T phase after the removal of the E field, and there are still some M_C phase regions that exist in the sample. It is important to estimate the contribution of the M_C phase to the dielectric and piezoelectric properties. If the phase structure is in the pure T phase after poling along $[011]_C$, the ideal intrinsic dielectric constant and piezoelectric coefficient can be calculated according to the coordinate transformation based on the material constants of single domain samples [9,13]. On the $(100)_C$ plane, the orientation dependence of the intrinsic tetragonal piezoelectric coefficient d_{33}^{in} and dielectric constant $\varepsilon_{33}^{\mathrm{in}}$ can be calculated by the following formulas:

$$d_{33}^{\mathrm{in}} = \left(d_{31}^{\mathrm{sd}} + d_{15}^{\mathrm{sd}}\right)\cos\alpha\,\sin^2\alpha + d_{33}^{\mathrm{sd}}\cos^3\alpha, \tag{2}$$

$$\varepsilon_{33}^{\mathrm{in}} = \varepsilon_{33}^{\mathrm{sd}}\cos^2\alpha + \varepsilon_{11}^{\mathrm{sd}}\sin^2\alpha, \tag{3}$$

where α is the angle between the $[001]_C$ and the calculated direction. The material constants on the right-hand side are those of the single T-domain data, whereas d_{33}^{in} and $\varepsilon_{33}^{\mathrm{in}}$ are the calculated constants along the desired direction. The parameters of single T-domain crystals are determined by $[001]_C$-poled samples in which no phase transition happens during the poling process. The results are as follows: $d_{33}^{\mathrm{sd}} = 307\,\mathrm{pC/N}$, $d_{31}^{\mathrm{sd}} = -134\,\mathrm{pC/N}$, $d_{15}^{\mathrm{sd}} = 1410\,\mathrm{pC/N}$, $\varepsilon_{33}^{\mathrm{sd}} = 775$, and $\varepsilon_{11}^{\mathrm{sd}} = 12\,550$. For the $[011]_C$ direction, $\alpha = 45^\circ$. Based on Eqs. (2) and (3), d_{33}^{in} and $\varepsilon_{33}^{\mathrm{in}}$ are calculated to be 560 pC/N and 6663, respectively. The measured results for the two quantities are 1052 pC/N and 10 661, respectively, (shown in Table I), which are nearly two times as large as the calculated ones. The huge discrepancy between the measured and the calculated values cannot be merely ascribed by the domain-wall motions, which is believed to be very low according to the literature reports [9,29]. They should originate from the existence of the M_C phase. The piezoelectric and dielectric responses originate from both intrinsic and extrinsic contributions: The intrinsic contributions are from the atomic displacements within the unit cell, whereas the extrinsic contributions are ascribed to domain-wall motions. Here we consider the contributions of the M_C phase from both intrinsic and extrinsic aspects.

Based on the calculated results of the Landau-Ginsburg-Devonshire theory, the free-energy profile of the M phase is rather flat, meaning that the P_S is very sensitive to the E field.

Very small stimuli could produce a relatively large polarization rotation and strains, leading to high dielectric and piezoelectric effects [16,17,30]. This corresponds to the intrinsic mechanism of improved properties in the M_C phase. Our results indicate that the existence of the M_C phase results in very high intrinsic contributions.

The extrinsic response is related to the domain-wall motions, which can be further subdivided into reversible and irreversible movements. The contribution of the reversible domain is ignored in this discussion as reversible domain-wall movements are very small due to the energetically equivalent P_S states [31]. The nonlinear effect of dielectric and piezoelectric responses below the coercive field corresponds primarily to the irreversible movements of the domain walls. The continuous rotation of P_S vectors in the M_C phase may result in a high level of irreversible domain-wall motions. In this paper, we take the piezoelectric coefficient d_{33} as an example to carry out the analysis. Rayleigh analysis has been performed to describe the nonlinear effect and the contribution of irreversible domain-wall motions to the piezoelectric response,

$$S(E) = (d_{\text{init}} + \alpha E_0)E \pm \alpha\left(E_0^2 - E^2\right)/2, \tag{4}$$

$$d(E_0) = d_{\text{init}} + \alpha E_0, \tag{5}$$

where $S(E)$ is the E-field induced strain, E_0 is the amplitude of the bipolar E field, and d_{init} is the intrinsic portion of the piezoelectric coefficient. The Rayleigh parameter α is a measure of the irreversible domain-wall displacement, thus αE_0 represents the extrinsic contribution from irreversible domain-wall motions. The total piezoelectric coefficient $d_{33}(E_0)$ can be calculated from the peak to peak of the bipolar S-E loop. The E_0 dependence of d_{33} is shown in Fig. 7. The parameters d_{init} and α can be obtained by fitting the d_{33} curve using Eq. (5) to give: $d_{\text{init}} = 500\,\text{pm/V}$ and $\alpha = 276\,\text{cm/kV}$. The inset in Fig. 7 shows the comparison between the measured S-E loop and the calculated one using Eq. (4). The two loops coincide well with each other. The α value is much larger

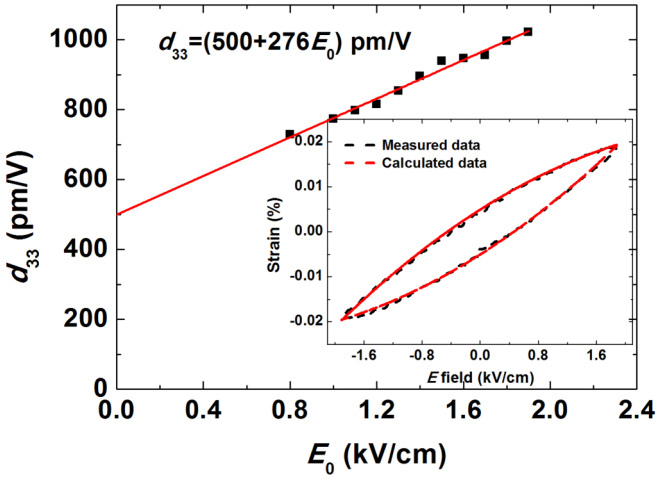

FIG. 7. E-field dependence of the piezoelectric coefficient d_{33} of a PMN-0.37PT single crystal at 1 Hz. The inset shows the comparison between the measured and the calculated strain vs E-field hysteresis loops.

than that in the $[001]_C$-orientated PMN-PT single crystal in the R and T compositional regions and is comparable to the highest value in the MPB composition, indicating a high level of irreversible domain-wall motions in the M_C phase [29]. The intrinsic piezoelectric response d_{init} is much lower than that in the $[001]_C$-orientated R and MPB crystals. The high-α and low-d_{init} values lead to high extrinsic contributions to the piezoelectric response, which is 35% at $E_0 = 1\,\text{kV/cm}$. Therefore, the M_C phase plays an important role in the high piezoelectric and dielectric properties through improving both the intrinsic and the extrinsic contributions.

It is of great interest to estimate the volume fractions of the T and M_C phases in the $[011]_C$-poled PMN-0.37PT single crystal. The piezoelectricity in the crystal should originate from the contribution of both T and M_C phases, therefore, the volume fractions may be estimated based on the effective piezoelectric coefficient. We assume that the volume fractions of the M_C and T phases are y and $1 - y$, respectively, and the following relationship may be used for this purpose:

$$d_{33}^T \times (1 - y) + d_{33}^M \times y = d_{33}^{\text{meas}}, \tag{6}$$

where d_{33}^T and d_{33}^M are the longitudinal piezoelectric coefficients of the tetragonal and M_C phases, respectively, and d_{33}^{meas} is the experimentally measured value in the domain-engineered state. It is reported that the extrinsic piezoelectric contribution in the pure tetragonal phase is very small whereas the intrinsic contribution is dominant [29,32]. Hence, it is reasonable to ignore the extrinsic contributions, so d_{33}^T should de be equal to d_{33}^{in} in Eq. (2), which is 560 pC/N. From Fig. 2, the piezoelectric coefficient d_{33}^M of the M_C phase can be estimated to be 4645 pC/N. The measured d_{33}^{meas} value is 1052 pC/N as listed in Table I. Based on Eq. (6), the volume fraction of the M_C phase is estimated to be ~12.0%, and the volume fraction of the T phase is ~88.0%.

C. Temperature dependence of phase structures and electromechanical properties

In order to investigate the phase stability of $[011]_C$-poled PMN-0.37PT single crystals, the temperature dependence of the domain structures is detected by the PLM, and the results are shown in Fig. 8. The sample has T and M_C phase coexistences at room temperature [Figs. 8(a) and 8(b)]. With the increase in temperature, the volume fraction of the T phase increases, which can be seen from the enlarged dark region at $\theta = 0°$ [Figs. 8(d) and 8(f)]. The coexistence of the M_C and T phases maintains until 175°C, above that the ferroelectric domains disintegrated and the system transformed to the cubic (C) phase for which the PLM show extinction at all angles [Figs. 8(g) and 8(h)]. A small fraction of the ferroelectric phase near the edge of the sample still exists due to internal stresses [the bright area in Fig. 8(h)]. As the temperature further increases to 190° C, the whole sample transforms into the C phase [Figs. 8(i) and 8(j)].

The temperature-dependent dielectric constant ε_{33}^T, lateral piezoelectric constant d_{31}, and electromechanical mechanical coupling factor k_{31} are measured as shown in Fig. 9. The Curie temperature T_C is 176 °C, coinciding with domain evolution measurement in Fig. 8. With a further increase in temperature, ε_{33}^T, d_{31}, and k_{31} all decrease gradually. There are two main

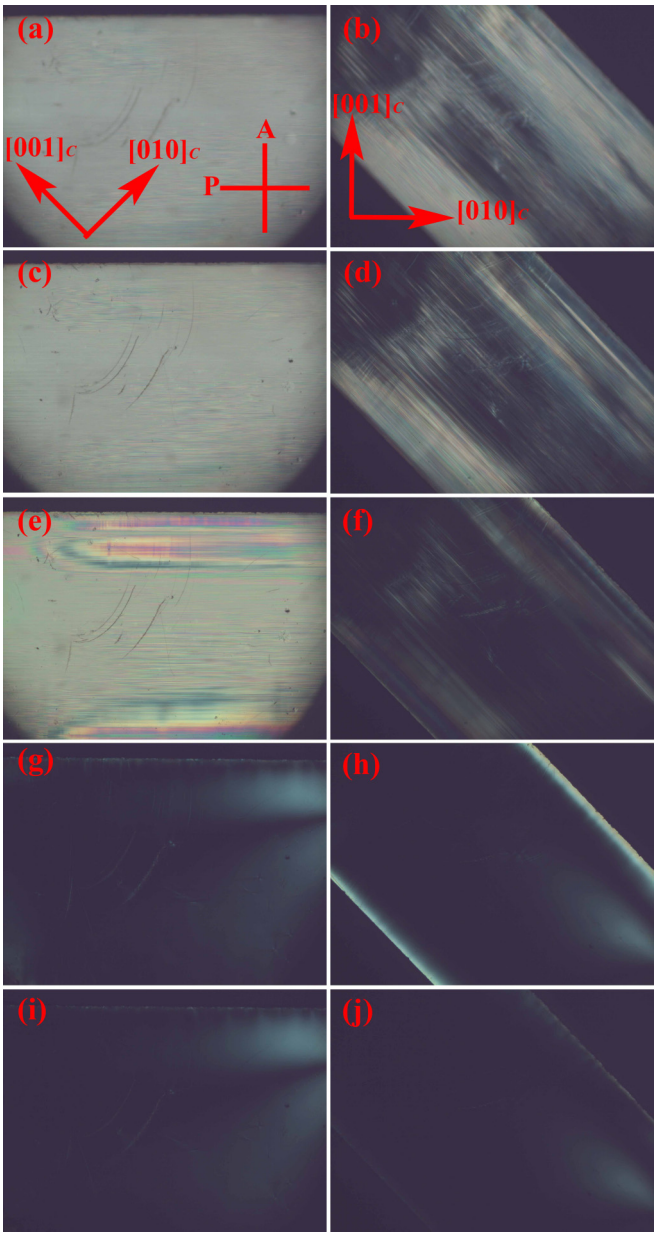

FIG. 8. Temperature dependence of domain configurations during heating process. (a) and (b) 25 °C, (c) and (d) 100 °C, (e) and (f) 175 °C, (g) and (h) 180 °C, and (i) and (j) 190 °C. Images in the left column were taken at $\theta = 45°$, whereas those in the right column were taken at $\theta = 0°$.

reasons causing the decrease in d_{31}, k_{31}, and ε_{33}^{T}. The first is the instability of the phase structures. As mentioned above, the $[011]_C$-poled PMN-0.37PT single crystal shows coexistence of the M_C and T phases, and the M_C phase contributes a lot to the high dielectric and piezoelectric properties. That is to say, larger M_C volume fractions lead to higher functional properties. As shown in Fig. 8, with the increase in temperature, the volume fraction of the T phase increases whereas that of the M_C phase decreases. The reduction in the M_C phase volume fraction results in the decrease in electric and electromechanical properties. The second is the intrinsic

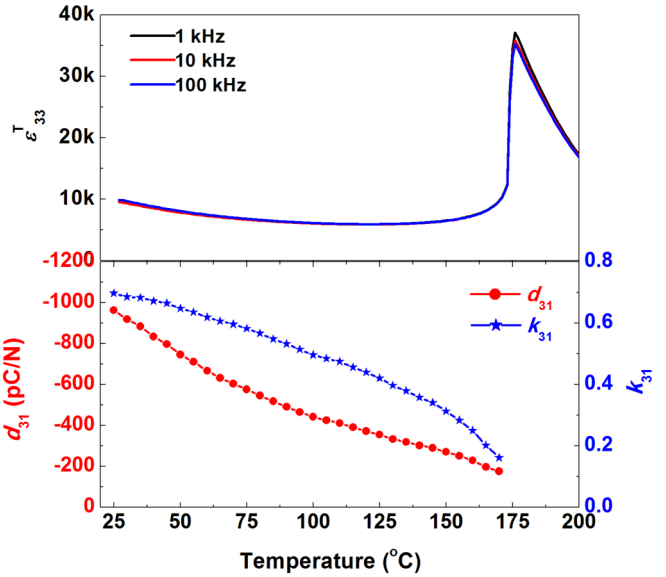

FIG. 9. The constants ε_{33}^{T}, d_{31}, and k_{31} of the $[011]_C$-poled PMN-0.37PT as a function of temperature.

contributions from the T phase, which also decreases with temperature. From coordinate transformation, the intrinsic piezoelectric constant d_{31}^{in} and $\varepsilon_{33}^{\text{in}}$ of the $[011]_C$-poled T-phase sample can be written as

$$d_{31}^{\text{in}} = \frac{\sqrt{2}}{4}\left(d_{31}^{\text{sd}} + d_{33}^{\text{sd}} - d_{15}^{\text{sd}}\right), \tag{7}$$

$$\varepsilon_{33}^{\text{in}} = \frac{1}{2}\left(\varepsilon_{11}^{\text{sd}} + \varepsilon_{33}^{\text{sd}}\right). \tag{8}$$

As mentioned above, d_{33}^{sd} and d_{31}^{sd} are much lower than d_{15}^{sd}, so d_{31}^{in} depends mainly on the d_{15}^{sd} value of the single domain state. Similarly, $\varepsilon_{11}^{\text{sd}}$ is much higher than $\varepsilon_{33}^{\text{sd}}$, so the dielectric constant $\varepsilon_{33}^{\text{in}}$ in the $[011]_C$-poled samples depends greatly on $\varepsilon_{11}^{\text{sd}}$. According to the literature, d_{15}^{sd} and $\varepsilon_{11}^{\text{sd}}$ decrease gradually with temperature in the T-phase temperature range [33]. As a result, the intrinsic d_{31}^{in} and $\varepsilon_{33}^{\text{in}}$ along $[011]_C$ decrease with temperature.

IV. SUMMARY AND CONCLUSIONS

To summarize, we have intensively investigated the phase-transition behavior of a tetragonal PMN-0.37PT single crystal driven by both the E field and the temperature and measured the full tensor properties of the $[011]_C$-poled PMN-0.37PT domain-engineered single crystal. The unpoled PMN-0.37PT single crystal is in the T phase at room temperature. Under an E field along $[011]_C$, the crystal undergoes the following phase-transition sequence: $T \rightarrow M_C \rightarrow O$ with an increase in the E field and $O \rightarrow M_C \rightarrow M_C + T$ in the decreasing process of the E field back to 0. The $[011]_C$-poled PMN-0.37PT single crystals show high longitudinal dielectric constants, piezoelectric coefficients, and electromechanical coupling factors, which can be attributed to the existence of the M_C phase.

With the increase in temperature, the volume fraction of the T phase increases at the expense of the M_C phase, and

the crystal finally transforms into the C phase at T_C (around 176°C). The dielectric, piezoelectric,and electromechanical properties all decrease gradually with temperature below T_C. The decrease in electrical and electromechanical properties should be mainly ascribed to the reduction of the volume percentage of the M_C phase, which has much larger functional properties.

ACKNOWLEDGMENTS

This work was supported by the National Key Basic Research Program of China (Grant No. 2013CB632900), the NIH under Grant No. P41-EB21820, the PIRS of HIT (Grant No. B201509), and the National Science Foundation of China (Grants No. 51572055 and No. 11372002).

[1] L. Zheng, X. Lu, H. Shang, Z. Xi, R. Wang, J. Wang, P. Zheng, and W. Cao, Phys. Rev. B **91**, 184105 (2015).
[2] R. Zhang, B. Jiang, W. Jiang, and W. Cao, Mater. Lett. **57**, 1305 (2003).
[3] J. M. Kiat, Y. Uesu, B. Dkhil, M. Matsuda, C. Malibert, and G. Calvarin, Phys. Rev. B **65**, 064106 (2002).
[4] H. Uršič, J. Tellier, J. Holc, S. Drnovšek, and M. Kosec, J. Eur. Ceram. Soc. **32**, 449 (2012).
[5] L. Zheng, R. Sahul, S. Zhang, W. Jiang, S. Li, and W. Cao, J. Appl. Phys. **114**, 104105 (2013).
[6] S. Zhang and F. Li, J. Appl. Phys. **111**, 031301 (2012).
[7] H. Cao, V. H. Schmidt, R. Zhang, W. Cao, and H. Luo, J. Appl. Phys. **96**, 549 (2004).
[8] F. Li, S. Zhang, Z. Xu, X. Wei, J. Luo, and T. R. Shrout, J. Appl. Phys. **107**, 054107 (2010).
[9] F. Li, S. Zhang, Z. Xu, X. Wei, J. Luo, and T. R. Shrout, J. Am. Ceram. Soc. **93**, 2731 (2010).
[10] L. Zheng, X. Huo, R. Wang, J. Wang, W. Jiang, and W. Cao, CrystEngComm **15**, 7718 (2013).
[11] R. Zhang, B. Jiang, W. Jiang, and W. Cao, Appl. Phys. Lett. **89**, 242908 (2006).
[12] X. Huo, S. Zhang, G. Liu, R. Zhang, J. Luo, R. Sahul, W. Cao, and T. R. Shrout, J. Appl. Phys. **112**, 124113 (2012).
[13] L. Zheng, S. Li, S. Sang, J. Wang, X. Huo, R. Wang, Z. Yuan, and W. Cao, Appl. Phys. Lett. **105**, 212902 (2014).
[14] S. Zhang, F. Li, J. Luo, R. Xia, W. Hackenberger, and T. R. Shrout, Appl. Phys. Lett. **97**, 132903 (2010).
[15] M. Davis, M. Budimir, D. Damjanovic, and N. Setter, J. Appl. Phys. **101**, 054112 (2007).
[16] D. Damjanovic, J. Am. Ceram. Soc. **88**, 2663 (2005).
[17] D. Damjanovic, Appl. Phys. Lett. **97**, 062906 (2010).
[18] R. Guo, L. E. Cross, S. E. Park, B. Noheda, D. E. Cox, and G. Shirane, Phys. Rev. Lett. **84**, 5423 (2000).
[19] B. Noheda, D. E. Cox, G. Shirane, J. Gao, and Z. G. Ye, Phys. Rev. B **66**, 054104 (2002).
[20] R. R. Chien, V. H. Schmidt, C. S. Tu, L. W. Hung, and H. Luo, Phys. Rev. B **69**, 172101 (2004).
[21] A. K. Singh and D. Pandey, Phys. Rev. B **67**, 064102 (2003).
[22] B. Noheda, D. E. Cox, G. Shirane, S. E. Park, L. E. Cross, and Z. Zhong, Phys. Rev. Lett. **86**, 3891 (2001).
[23] X. Huo, R. Zhang, L. Zheng, S. Zhang, R. Wang, J. Wang, S. Sang, B. Yang, and W. Cao, J. Am. Ceram. Soc. **98**, 1829 (2015).
[24] R. Zhang, B. Jiang, and W. Cao, J. Appl. Phys. **90**, 3471 (2001).
[25] X. Liu, S. Zhang, J. Luo, T. R. Shrout, and W. Cao, J. Appl. Phys. **106**, 074112 (2009).
[26] X. Zhao, B. Fang, H. Cao, Y. Guo, and H. Luo, Mater. Sci. Eng., B **96**, 254 (2002).
[27] E. Sun, W. Cao, W. Jiang, and P. Han, Appl. Phys. Lett. **99**, 032901 (2011).
[28] S. Zhang, C. A. Randall, and T. R. Shrout, J. Appl. Phys. **95**, 4291 (2004).
[29] F. Li, S. Zhang, Z. Xu, X. Wei, J. Luo, and T. R. Shrout, J. Appl. Phys. **108**, 034106 (2010).
[30] X. Lu, L. Zheng, H. Li, and W. Cao, J. Appl. Phys. **117**, 134101 (2015).
[31] S. Li, W. Cao, and L. E. Cross, J. Appl. Phys. **69**, 7219 (1991).
[32] R. E. Eitel, T. R. Shrout, and C. A. Radall, J. Appl. Phys. **99**, 124110 (2006).
[33] F. Li, S. Zhang, Z. Xu, X. Wei, and T. R. Shrout, Adv. Funct. Mater. **21**, 2118 (2011).